Chemical Physics 373 (2010) 145–152

Contents lists available at ScienceDirect

Chemical Physics

journal homepage: www.elsevier.com/locate/chemphys

Mechanism enabling the observation of the formally optically-forbidden $2A_g^-$ and $1B_u^-$ states in resonance-Raman excitation profiles of spheroidene in KBr disc

Hiroyoshi Nagae [a,*], Yasushi Koyama [b]

[a] Kobe City University of Foreign Studies, Gakuen-Higashimachi, Nishi-ku, Kobe 651-2187, Japan
[b] Faculty of Science and Technology, Kwansei Gakuin University, Gakuen, Sanda 669-1337, Japan

ARTICLE INFO

Article history:
Received 21 November 2009
In final form 25 May 2010
Available online 8 June 2010

Keywords:
Carotenoids
Optically-forbidden excited state
Resonance-Raman excitation profile
Self-absorption
Spheroidene
KBr disc

ABSTRACT

An expression for the Albrecht A-term resonance-Raman excitation profiles (RREP) of a pigment dispersed in a KBr disc, in such a way that the pigment molecules aggregate in a microcrystal and the microcrystals are dispersed in the KBr disc, is formulated by taking into account the self-absorption of incident and scattered light and the distribution of microcrystals properly. Based on the resultant formula, simulations for the RREPs of spheroidene dispersed in KBr disc were carried out in the spectral region from 12,000 to 24,000 cm^{-1}. Fairly good agreement between the simulations and the observed RREPs was obtained for different concentrations of spheroidene. Mechanisms have been investigated which enable the observation of the formally optically-forbidden (very weakly allowed) $2A_g^-$ and $1B_u^-$ states of spheroidne in RREPs free from the contribution of the optically-allowed $1B_u^+$ state, and a two-step self-absorption mechanism is proposed.

1. Introduction

Carotenoids function as an important light harvester and a quencher of excess excitation energy in photosynthetic organisms [1,2]. Detailed knowledge of their excited states is of primary importance. Due to the approximate C_{2h} symmetry of their conjugated polyene chain, the lower electronic excited states of carotenoids can be labeled by the C_{2h} symmetry group representations. The strongest absorption is ascribable to the electronic transition from the ground $\left(1A_g^-\right)$ to the $1B_u^+$ state, where an additional index, − or +, reflects the alternacy particle–hole symmetry [transition dipole moments between states having the same alternacy symmetry vanish in the Pariser-Parr-Pople (PPP) approximation] [3]. The lowest singlet excited state which is optically-forbidden is assigned to $2A_g^-$ [4].

It has been theoretically predicted by Tavan and Schulten [5] (based on the extrapolation of the multireference single and double excitation configuration-interaction in PPP Hamiltonian (PPP-MRD-CI) calculations) and by Kurashige et al. [6] (by using multireference Mϕller-Plesset (MRMP) method based on the complete active-space configuration-interaction (CASCI) reference functions) that there are additional formally optically-forbidden excited $1B_u^-$ and $3A_g^-$ states between the $2A_g^-$ and $1B_u^+$ states for longer polyenes having more than 7 and 11 conjugated double bonds, respectively. However, their presence has not been generally accepted.

Sashima et al. [7] found, in 1999 (Fig. 1), a new peak in the resonance-Raman excitation profiles (RREP) of the a_g-type C=C and C—C stretching modes between the positions of $2A_g^-$ and $1B_u^+$ states for crystalline spheroidene dispersed in KBr disc at 77 K. By increasing the concentration of the carotenoid starting from 1.6×10^{-5} M, they found the RREP peak appearing at a concentration of 8.0×10^{-3} M.

RREP measurement had been already proved to be a reliable method to determine the energy of the 'optically-forbidden' $2A_g^-$ state of carotenoids in a single crystal [8], randomly oriented crystals [9] and polycrystalline films [10]. The coincidence of the peak positions of the lowest-energy peaks for the C=C and C—C vibrational modes at 14,200 cm^{-1} for $2A_g^-$ states (see Fig. 1(c)) and their characteristic vibrational progressions made the last authors to conclude that the RREPs originate from the *A* term in the Albrecht theory [11]. This observation indicates that the transition dipole moment between the $2A_g^-$ and $1A_g^-$ (ground) states is actually not zero. This was later confirmed by fluorescence spectroscopy [12] and the transition dipole moment was determined to be about 5% of the $1B_u^+ \leftarrow 1A_g^-$ transition dipole moment [13]. Based on the same reason, Sashima et al. [7] ascribed the newly discovered RREP peak in-between the $2A_g^-$ and $1B_u^+$ states to the $1B_u^- \leftarrow 1A_g^-$ electronic excitation according to the aforementioned theoretical prediction by Tavan and Schulten.

Furthermore, they ascribed the appearance of the $1B_u^-$ RREP peaks at a concentration of 8.0×10^{-3} M completely free from the contribution of the $1B_u^+$ RREP, to the self-absorption effect, which strongly suppresses the $1B_u^+$ RREP. However, we have found

* Corresponding author. Tel.: +81 78 794 8225; fax: +81 78 792 9020.
E-mail address: hf_nagae@inst.kobe-cufs.ac.jp (H. Nagae).

0301-0104/$ - see front matter © 2010 Elsevier B.V. All rights reserved.
doi:10.1016/j.chemphys.2010.05.030

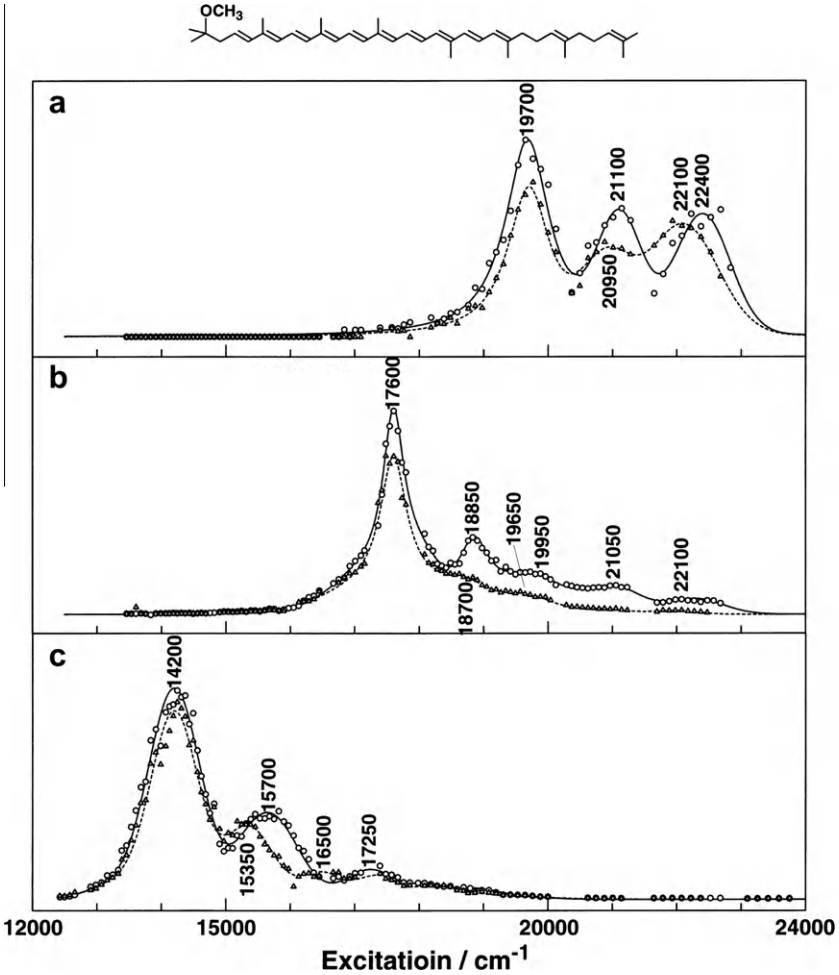

Fig. 1. The molecular structure of all-*trans*-spheroidene (top) and the resonance-Raman excitation profiles of the C=C (○) and the C—C (△) stretching modes for (a) 1.6×10^{-5} M spheroidene in KBr disc recorded in the geometry of grazing-incidence and 90°-scattering; (b) 8.0×10^{-3} M spheroidene in KBr disc recorded in the back-scattering geometry; (c) spheroidene crystals in a film recorded in the grazing-incidence and 90°-scattering geometry [7].

that the experimental result can not be explained theoretically, if we assume that the carotenoid molecules are uniformly dispersed in the KBr disc. The reason is as follows: Let us first consider an infinitely deep KBr 'disc' or cylinder. The penetration length of incident light is roughly inversely proportional to the square of the relevant transition dipole moment according to the Lambert–Beer law. On the other hand the RREP intensity of each molecule is proportional to the fourth power of it. Thus, the overall RREP intensity from the 'disc' is proportional to the square of the transition dipole moment and, as a result the RREP associated with a weak transition dipole moment should never dominates the one associated with a strong transition dipole moment. For a finite depth of disc, the above rule applies also safely, since the number of weak absorptive molecules which participate in RR scattering in the disc is less than that of molecules in the penetration region in the hypothetical infinitely deep KBr 'disc'.

Fig. 2 presents pictures of anhydrorhodovibrin ($C_{41}H_{58}O$) particles in KBr disc at concentrations of 4×10^{-3} M (a,b,c,d) and 7×10^{-5} M (e, f). Obviously the carotenoid molecules are dispersed not as single molecules but as particles of carotenoid aggregates. The situation will also applies to spheroidene, since the molecular structure of spheroidene ($C_{41}H_{60}O$) is almost the same as anhydrorhodovibrin ($C_{41}H_{58}O$).

Thus, it is worthwhile to simulate theoretically the RREP by taking into account this unique arrangement of the carotenoid molecules in KBr disc and investigate the mechanism by which the formally optically-forbidden $2A_g^-$ and $1B_u^-$ states of carotenoids are observed in RREPs free from the contribution of the optically-allowed $1B_u^+$ state. This paper is organized as follows: Following this introduction section, a simple model is presented in Section 2 to formulate the RREPs of a pigment in KBr disc, where (i) the aggregates are regarded as microcrystals with an equal size, and (ii) two kinds of self-absorptions are considered. In Section 3, the result of simulations of the RREPs for spheroidene dispersed in KBr disc, based on the formula obtained in Section 2, will be presented. Finally, discussion will be in Section 4.

2. Theory

Let us examine a KBr disc, in which aggregated particles of spheroidene are dispersed (Fig. 3). The thickness of the disc is l. The disc is placed on a perfect absorptive plate at $x = l$. Incident light with frequency ν (in units of cm^{-1}) and intensity $I_0(\nu)$ is perpendicular to the surface of the disc and the RR scattering $I_R(\nu - \vec{\nu}^{(0)} \cdot \vec{u})$ is recorded by the use of back-scattering geometry. The concentration of the pigment in the disc, i.e., the total number of the pigment molecules divided by the volume of disc, is denoted by $\bar{n}(\bar{n} = N_A \times C/10^3$, where C is molarity and N_A is Avogadro's number). We also refer to $\bar{n}$ as the overall concentration of the pigment in the disc.

We assume that the vibronic states of the molecule can be described by the adiabatic Born–Oppenheimer products; in the

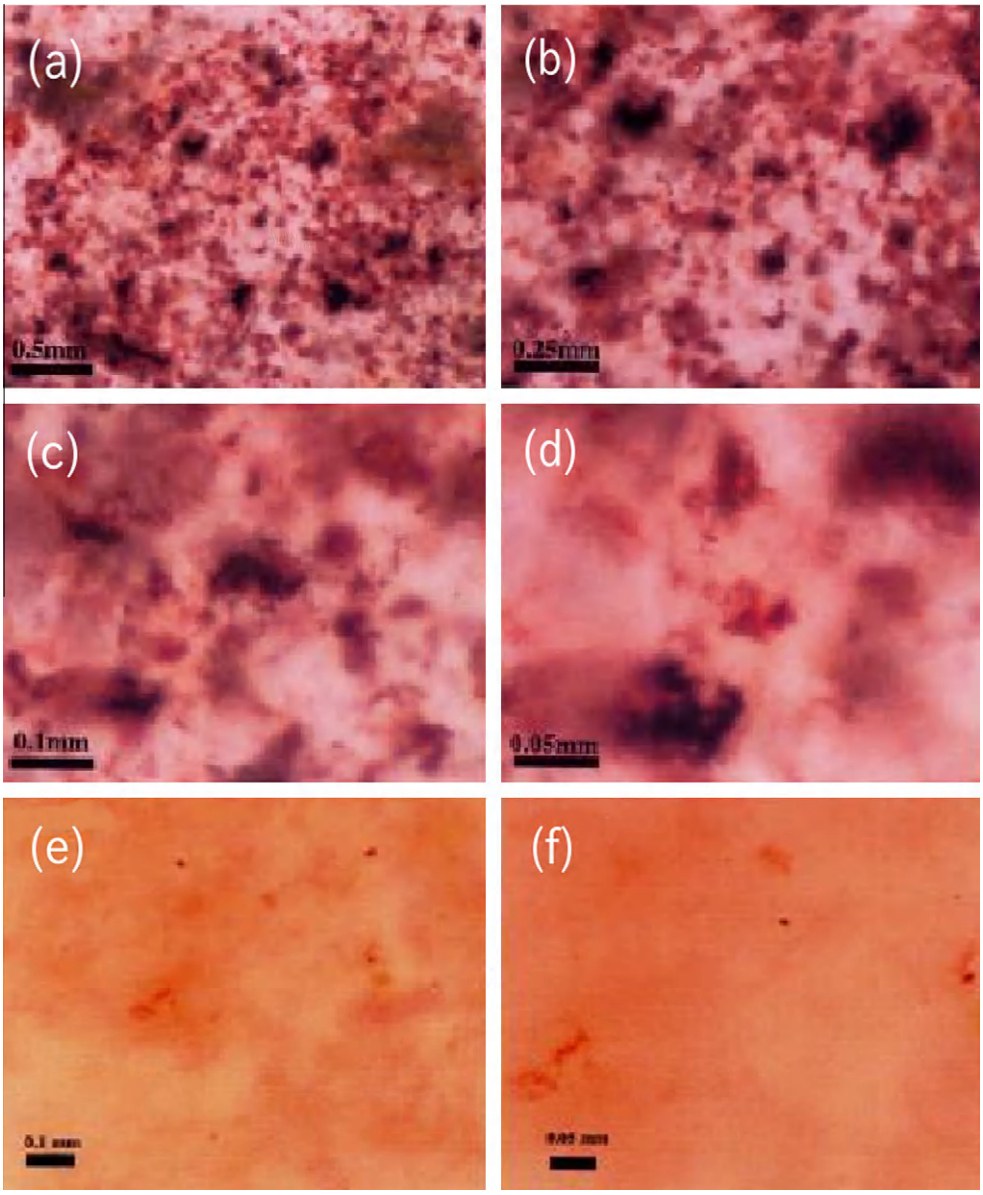

Fig. 2. Pictures of aggregates of molecules of anhydrorhodovibrin in KBr disc at 4×10^{-3} M for a, b, c, d and at 7×10^{-5} M for e, f. Scale bars are 0.5 mm, 0.25 mm 0.1 mm and 0.05 mm, respectively for a, b, (c, e) and (d, f). Courtesy of Dr. K. Furuichi.

ground (kth excited) electronic state, the vibronic wave functions can be written as $|\psi_0\rangle|\chi_{\vec{u}}^{(0)}\rangle(|\psi_k\rangle|\chi_{\vec{v}}^{(k)}\rangle)$. Here, $|\psi_0\rangle$ and $|\psi_k\rangle$ are the electronic wavefunctions whereas $|\chi_{\vec{u}}^{(0)}\rangle$ and $|\chi_{\vec{v}}^{(k)}\rangle$ are the vibrational wavefunctions. The vibrational wavefunctions are taken as the products of harmonic oscillators:

$$|\chi_{\vec{u}}^{(0)}\rangle = \prod_i |\chi_{u_i}^{(0)}\rangle, \quad |\chi_{\vec{v}}^{(k)}\rangle = \prod_i |\chi_{v_i}^{(k)}\rangle. \tag{1}$$

where u_i (v_i) is the vibrational quantum number of the ith vibrational mode in the ground (excited) state. Their vibrational frequencies in the ground and the kth excited states are $\vec{\nu}^{(0)} = (\nu_1^{(0)}, \nu_2^{(0)}, \cdots)$ and $\vec{\nu}^{(k)} = (\nu_1^{(k)}, \nu_2^{(k)}, \cdots)$, respectively. $\vec{0} - \vec{0}$ excitation energy (frequency) of the kth state is denoted by ν_{k0}.

For the spontaneous or incoherent RR transition $\vec{u} \leftarrow \vec{0}$, we assume that the A-term of the Albrecht theory is applicable. Then, the orientationally-averaged RR scattering tensor is given as [14]

$$\alpha_{\vec{u}\vec{0}} = \sum_k \alpha_{\vec{u}\vec{0}}^{(k)}, \tag{2}$$

with

$$\alpha_{\vec{u}\vec{0}}^{(k)} = \frac{1}{3hc} \sum_{\vec{v}} d_{k0}^2 \frac{\left\langle \chi_{\vec{u}}^{(0)} | \chi_{\vec{v}}^{(k)} \right\rangle \left\langle \chi_{\vec{v}}^{(k)} | \chi_{\vec{0}}^{(0)} \right\rangle}{\nu_{k0} + \vec{\nu}^{(k)} \cdot \vec{v} - \nu - i\gamma_{k0}}, \tag{3}$$

where h is Planck's constant, c the velocity of light, d_{k0} the transition dipole moment evaluated at the equilibrium geometry of the ground state (i.e., $d_{k0} = |\langle \psi_k | \vec{d} | \psi_0 \rangle|$, where $\vec{d}$ is the dipole operator) and γ_{k0} is the homogeneous dephasing constant for the electronic coherence between the kth excited and the ground states. γ_{k0} is related to the decay constant for the kth excited state, γ_k, as

$$\gamma_{k0} = \gamma_k/2 + \hat{\Gamma}_{k0}, \tag{4}$$

where $\hat{\Gamma}_{k0}$ is the pure dephasing rate [15].

In order to simplify the simulation of the RREP, we regard the aggregated particles as microcrystals which are homogeneous with a size 'a' (set to the average length of the particles), irrespective of the overall concentration of pigment (see Fig. 2). Let us first consider the RR scattering from a microcrystal. Due to the self-absorp-

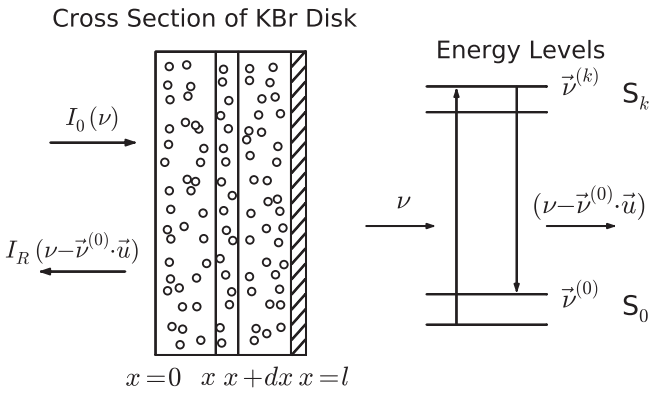

Fig. 3. Geometry of a KBr disc (left) in which aggregated particles of spheroidene are dispersed, and an energy-level diagram for spontaneous Raman scattering process (right). $I_0(\nu)$ is the intensity of incident light with frequency ν and $I_R(\nu-\vec{\nu}^{(0)}\cdot\vec{u})$ the intensity of resonance-Raman scattering with frequency $(\nu-\vec{\nu}^{(0)}\cdot\vec{u})$. S_0 and S_k represent the ground and the kth excited states ($S_1 = 2A_g^-$, $S_2 = 1B_u^-$ and $S_3 = 1B_u^+$). $\vec{\nu}^{(0)}(\vec{\nu}^{(k)})$ represents a set of vibrational frequencies of the ground (kth excited) state and $\vec{u}$ represents a set of vibrational quantum numbers in the ground state after Raman scattering.

tion within microcrystal, based on the Lambert–Beer law, we find that the RR (back-) scattering intensity from a microcrystal associated with the kth excited state is proportional to

$$\left|\alpha_{\vec{u}\vec{0}}^{(k)}\right|^2 a^2 \int_0^a \exp\left\{-\left[\sigma_k(\nu)+\sigma_k(\nu-\vec{\nu}^{(0)}\cdot\vec{u})\right]n_c x\right\} n_c\, dx, \tag{5}$$

where $\sigma_k(\nu)$ is the absorption cross section due to the kth excitation and n_c is the number density of the pigment molecules in the microcrystal. Here, no reflection on the surface is assumed. For simplicity, we approximate this by

$$\left|\alpha_{\vec{u}\vec{0}}^{(k)}\right|^2 a^2 \int_0^a \exp(-\bar{\sigma}_k n_c x) n_c\, dx = \frac{\left|\alpha_{\vec{u}\vec{0}}^{(k)}\right|^2 a^2}{\bar{\sigma}_k}\left[1-\exp(-\bar{\sigma}_k n_c a)\right], \tag{6}$$

where $\bar{\sigma}_k$ is the absorption cross section at $\nu = \nu_{k0}[\bar{\sigma}_k = 3.82\times 10^{-21}\epsilon(\nu_{k0})$ in cgs units, where $\epsilon(\nu)$ is the molar extinction coefficient [16]; note that $\sigma_k(\nu_{k0}-\vec{\nu}^{(0)}\cdot\vec{u})\approx 0$ for $\vec{u}\neq\vec{0}$]. We rewrite this expression as

$$\left|r_k\alpha_{\vec{u}\vec{0}}^{(k)}\right|^2 a^3 n_c \quad \text{with} \quad r_k = \sqrt{\frac{1-\exp(-\bar{\sigma}_k n_c a)}{\bar{\sigma}_k n_c a}}. \tag{7}$$

Denoting the intensity of incident light at the position of the microcrystal by $I(\nu)$, $I(\nu)\left|r_k\alpha_{\vec{u}\vec{0}}^{(k)}\right|^2 a^3 n_c$ gives exactly the Raman intensity from the microcrystal for $\nu = \nu_{k0}$ except certain factors, while it gives rough estimate of the Raman intensity for $\nu\neq\nu_{k0}$. Since $a^3 n_c$ is the number of molecules in the microcrystal, r_k^2 represents the RR scattering efficiency per molecule (r_k is referred to as the square root of the RR scattering efficiency). The stronger the self-absorption or the larger the absorption cross section of the kth electronic transition becomes, the smaller the value of r_k becomes. With decreasing (increasing) size of the microcrystal, the value of r_k approaches 1 $(1/\sqrt{\bar{\sigma}_k n_c a})$; when there are no aggregates, $r_k = 1$. We refer to the self-absorption associated with the pigment density in microcrystal, n_c, as the first kind of self-absorption in the present paper. It should be noted that the same expression holds in the case when incident light creates an exciton, so long as the delocalization length of exciton is much smaller than the size of microcrystal.

Considering excited states simultaneously, the RR (back-) scattering intensity from a microcrystal is proportional to

$$S_{\vec{u}\vec{0}}(\nu)a^3 n_c \quad \text{with} \quad S_{\vec{u}\vec{0}}(\nu) = \left|\sum_k r_k\alpha_{\vec{u}\vec{0}}^{(k)}\right|^2. \tag{8}$$

Substituting Eq. (3) in the last equation, we have

$$S_{\vec{u}\vec{0}}(\nu) = \frac{1}{9h^2c^2}\left(\sum_k\sum_{\vec{v}} r_k d_{k0}^2 \frac{\left\langle\chi_{\vec{u}}^{(0)}|\chi_{\vec{v}}^{(k)}\right\rangle\left\langle\chi_{\vec{v}}^{(k)}|\chi_{\vec{0}}^{(0)}\right\rangle}{\nu_{k0}+\vec{\nu}^{(k)}\cdot\vec{v}-\nu-i\gamma_{k0}}\right) \times\left(\sum_{k'}\sum_{\vec{v}'} r_{k'} d_{k'0}^2 \frac{\left\langle\chi_{\vec{0}}^{(0)}|\chi_{\vec{v}'}^{(k')}\right\rangle\left\langle\chi_{\vec{v}'}^{(k')}|\chi_{\vec{u}}^{(0)}\right\rangle}{\nu_{k'0}+\vec{\nu}^{(k')}\cdot\vec{v}'-\nu+i\gamma_{k'0}}\right). \tag{9}$$

Now, we assume that the overlap of $\alpha_{\vec{u}\vec{0}}^{(k)}$ and $\alpha_{\vec{u}\vec{0}}^{(k')}(k\neq k')$ as functions of ν (the incident light frequency) can be neglected and further assume that terms having different values of $\vec{v}$ and $\vec{v}'$ is negligibly small, this condition being realized when $\gamma_{k0}\lesssim|\nu_i^{(k)}-\nu_j^{(k)}|(i\neq j)$. Then, Eq. (9) reduces to

$$S_{\vec{u}\vec{0}}(\nu) = \frac{1}{9h^2c^2}\sum_k\sum_{\vec{v}} r_k^2 d_{k0}^4 \frac{\left|\left\langle\chi_{\vec{u}}^{(0)}|\chi_{\vec{v}}^{(k)}\right\rangle\left\langle\chi_{\vec{v}}^{(k)}|\chi_{\vec{0}}^{(0)}\right\rangle\right|^2}{\left(\nu_{k0}+\vec{\nu}^{(k)}\cdot\vec{v}-\nu\right)^2+\gamma_{k0}^2}. \tag{10}$$

Inhomogeneous environment of the pigment molecule affects the RR scattering tensor by changing the excitation energies ν_{k0}. We assume, for simplicity, that the environment causes the same energy change for all the excited states and that the distribution of the effect is represented by a Gaussian function. Then, $S_{\vec{u}\vec{0}}(\nu)$ is modified into

$$S_{\vec{u}\vec{0}}(\nu) = \frac{1}{9h^2c^2}\sum_k\sum_{\vec{v}}\int_{-\infty}^{\infty} r_k^2 d_{k0}^4 \frac{\left|\left\langle\chi_{\vec{u}}^{(0)}|\chi_{\vec{v}}^{(k)}\right\rangle\left\langle\chi_{\vec{v}}^{(k)}|\chi_{\vec{0}}^{(0)}\right\rangle\right|^2}{\left(\overline{\nu}_{k0}+\vec{\nu}^{(k)}\cdot\vec{v}-\nu-\nu'\right)^2+\gamma_{k0}^2} \times\frac{1}{\sqrt{2\pi\Delta_{\text{in}}^2}}\exp\left(-\frac{\nu'^2}{2\Delta_{\text{in}}^2}\right)d\nu', \tag{11}$$

where $\overline{\nu}_{k0}$ is the average of the kth excitation energy in the different environment and Δ_{in} is the root mean square amplitude of the inhomogeneous frequency fluctuation. The integral on the right-hand side can be performed to yield

$$S_{\vec{u}\vec{0}}(\nu) = \frac{\pi}{9h^2c^2}\sum_k\sum_{\vec{v}}\frac{r_k^2 d_{k0}^4}{\gamma_{k0}}\left|\left\langle\chi_{\vec{u}}^{(0)}|\chi_{\vec{v}}^{(k)}\right\rangle\left\langle\chi_{\vec{v}}^{(k)}|\chi_{\vec{0}}^{(0)}\right\rangle\right|^2 \times f_V\left[\left(\overline{\nu}_{k0}+\vec{\nu}^{(k)}\cdot\vec{v}-\nu\right),\Delta_{\text{in}},\gamma_{k0}\right], \tag{12}$$

where $f_V(x,\Delta_{\text{in}},\gamma_{k0})$ is the so-called Voigt profile and is defined by

$$f_V(x,\Delta_{\text{in}},\gamma_{k0}) = \frac{1}{\sqrt{2\pi}\Delta_{\text{in}}}K\left(\frac{x}{\sqrt{2}\Delta_{\text{in}}},\frac{\gamma_{k0}}{\sqrt{2}\Delta_{\text{in}}}\right), \tag{13}$$

with

$$K(x,y) = \text{Re}\{\exp[-(x+iy)^2]\text{erfc}[-i(x+iy)]\}. \tag{14}$$

Here, erfc (z) is the complementary complex error function [$\text{erfc}(z) = (2/\sqrt{\pi})\int_z^\infty e^{-t^2}dt$] and Re means taking the real part. The full-width at half-maxima (FWHM) of Voigt profile is given as

$$\text{FWHM}_V \approx 2\times 0.51346\gamma_{k0} + \sqrt{4\times 0.2169\gamma_{k0}^2 + 8\ln(2)\Delta_{\text{in}}^2}, \tag{15}$$

with 0.02% accuracy [17]. The Voigt profile $f_V(x,\Delta_{\text{in}},\gamma_{k0})$ takes its maximal value at $x = 0$ which is given from Eqs. (13) and (14) as

$$\max\text{of } f_V = \frac{1}{\sqrt{2\pi\Delta_{\text{in}}^2}}\exp\left(\frac{\gamma_{k0}^2}{2\Delta_{\text{in}}^2}\right)\text{erfc}\left(\frac{\gamma_{k0}}{\sqrt{2}\Delta_{\text{in}}}\right). \tag{16}$$

By using Eqs. (15) and (16), we find that the Voigt profiles $f_V(x,\Delta_{\text{in}},\gamma_{k0})$ with the γ_{k0} to Δ_{in} ratio of 0.1, 0.5, 1.0, 1.5 and 2.0 can be approximated by the Gaussian profiles having a standard deviation of $1.08\Delta_{\text{in}}, 1.43\Delta_{\text{in}}, 1.91\Delta_{\text{in}}, 2.43\Delta_{\text{in}}$ and $2.97\Delta_{\text{in}}$, respectively; the maximal values of the two corresponding functions are equal and the FWHMs of the Gaussian profiles are about 8%, 15%, 25%, 32% and 36% larger than those of the corresponding Voigt pro-

files. Thus, neglecting small differences in the FWHMs between the two functions, we can approximate the Voigt profiles in Eq. (12) by appropriate Gaussian profiles, as far as we are interested in the overall shapes of RREPs. Further, for simplicity, we approximate them by the Gaussian profiles with the same standard deviation of s. Then, Eq. (12) can be approximated as

$$S_{\vec{u}\vec{0}}(\nu) = \frac{\pi}{9h^2c^2}\sum_k\sum_{\vec{v}}\frac{r_k^2 d_{k0}^4}{\gamma_{k0}}\left|\left\langle\chi_{\vec{u}}^{(0)}|\chi_{\vec{v}}^{(k)}\right\rangle\left\langle\chi_{\vec{v}}^{(k)}|\chi_{\vec{0}}^{(0)}\right\rangle\right|^2\times\frac{1}{\sqrt{2\pi s^2}} \times \exp\left[-\frac{(\nu-\overline{\nu}_{k0}-\vec{v}^{(k)}\cdot\vec{v})^2}{2s^2}\right]. \tag{17}$$

The absorption cross section of the pigment for a light with frequency ν is given by

$$\sigma(\nu) = \sum_k\frac{4\pi^2\nu}{3\hbar c}|d_{k0}|^2\sum_{\vec{v}}\left|\left\langle\chi_{\vec{0}}^{(0)}|\chi_{\vec{v}}^{(k)}\right\rangle\right|^2\times\frac{1}{\sqrt{2\pi s'^2}} \times \exp\left[-\frac{(\nu-\overline{\nu}_{k0}-\vec{v}^{(k)}\cdot\vec{v})^2}{2s'^2}\right], \tag{18}$$

where $\hbar = h/2\pi$ [16]. Here, we approximated the line shape functions by the Gaussian functions with the same standard deviation s' irrespective of the electronic state for the reason similar to the case in the RR scattering intensity.

So far, we have obtained expressions for the RR scattering from a microcrystal ($\propto S_{\vec{u}\vec{0}}(\nu)a^3n_c$) and the absorption cross section of the pigment ($\sigma(\nu)$). The observed RR transition $\vec{u}\leftarrow\vec{0}, I_R(\nu-\vec{v}^{(0)}\cdot\vec{u})$, can be regarded as the sum of RR scattering from all the microcrystals within the KBr disc. The contribution of a microcrystal placed at x (see Fig. 3) to the observed RR transition can be calculated as follows. Based on the Lambert–Beer law, the intensity of incident light at x is given by

$$I(\nu) = I_0(\nu)\exp\left[-\int_0^x\sigma(\nu)n(x')dx'\right], \tag{19}$$

where $n(x')$ is the number density of the pigment at x'. Assuming that the average particle-size (length), a, is much shorter than the thickness of the disc, l, i.e., $a \ll l$ and that the particles (microcrystals) are randomly dispersed in the disc, we can approximate $\int_0^x\sigma(\nu)n(x')dx'$ by $\sigma(\nu)\bar{n}x$, where $\bar{n}$ is the overall concentration of pigment in the disc. This leads to

$$I(\nu) = I_0(\nu)\exp[-\sigma(\nu)\bar{n}x]. \tag{20}$$

Thus, the RR scattering intensity from a microcrystal at x is proportional to

$$I_0(\nu)\exp[-\sigma(\nu)\bar{n}x]S_{\vec{u}\vec{0}}(\nu)a^3n_c. \tag{21}$$

Then, taking into account the self-absorption for the RR scattering light, we find that the contribution of the microcrystal to the observed RR transition is proportional to

$$I_0(\nu)\exp\left\{-[\sigma(\nu)+\sigma(\nu-\vec{v}^{(0)}\cdot\vec{u})]\bar{n}x\right\}S_{\vec{u}\vec{0}}(\nu)a^3n_c. \tag{22}$$

We call the self-absorption associated with the overall concentration (density), $\bar{n}$, the second kind of self-absorption in the present paper.

Summing up the contributions from all the microcrystals, we obtain the observed RR intensity of frequency $\nu-\vec{v}^{(0)}\cdot\vec{u}$ as

$$I_R(\nu-\vec{v}^{(0)}\cdot\vec{u}) = KI_0(\nu)(\nu-\vec{v}^{(0)}\cdot\vec{u})^4\times S_{\vec{u}\vec{0}}(\nu)\int_0^l \times\exp\left\{-[\sigma(\nu)+\sigma(\nu-\vec{v}^{(0)}\cdot\vec{u})]\bar{n}x\right\}\bar{n}\,dx, \tag{23}$$

where K is a constant and $S_{\vec{u}\vec{0}}(\nu)$ is defined by Eq. (17) [18]. Here, we approximate $\sum a^3n_c$ by $\int\bar{n}dx$ under the assumption of random dispersion of microcrystals in KBr disc. Carrying out the integration, we obtain

$$I_R(\nu-\vec{v}^{(0)}\cdot\vec{u}) = KI_0(\nu)(\nu-\vec{v}^{(0)}\cdot\vec{u})^4\times S_{\vec{u}\vec{0}}(\nu) \times\frac{1-\exp\{-[\sigma(\nu)+\sigma(\nu-\vec{v}^{(0)}\cdot\vec{u})]\bar{n}l\}}{\sigma(\nu)+\sigma(\nu-\vec{v}^{(0)}\cdot\vec{u})}. \tag{24}$$

The RREP is a plot of the ratio $I_R(\nu-\vec{v}^{(0)}\cdot\vec{u})/I_0(\nu)(\nu-\vec{v}^{(0)}\cdot\vec{u})^4$ versus ν.

3. Simulation

As stated in Introduction, the formally optically-forbidden $2A_g^-$ and $1B_u^-$ states of spheroidene have actually non zero transition dipole moments, probably due to lack of the perfect C_{2h} symmetry $\left(2A_g^-\right)$ or the approximate selection rule $\left(1B_u^-\right)$. (The selection rule due to the alternacy symmetry is not exact.) Therefore, the formula presented in Section 2, which is based on the A-term of Albrecht theory, will be applicable to the RREPs of spheroidene.

Then, based on the expression made in the previous section, i.e., Eq. (24) together with Eqs. (17) and (18), we performed the simulation of the RREPs of spheroidene dispersed in a KBr disc with overall concentrations of (a) 1.6×10^{-5} M, (b) 8×10^{-3} M, (c) $\lesssim 1.75\times10^{-1}$ M; the spectral region was taken from 12,000 cm^{-1} to 24,000 cm^{-1} which includes the electronic transitions from the $1A_g^-$ state to the $2A_g^-, 1B_u^-$ and $1B_u^+$ states (Fig. 5). In the following, the totally symmetric C=C and C–C stretching vibrational modes will be referred to as the first and second ones ($i = 1,2$) and the $1A_g^-, 2A_g^-, 1B_u^-$ and $1B_u^+$ states as S_0, S_1, S_2 and S_3. Moreover, the indexes i and k are used to indicate vibrational modes and electronic states, respectively.

For the simulations, the values of description parameters $s, s', \gamma_{k0}, r_k, d_{k0}, \nu_i^{(0)}, \nu_i^{(k)}, \overline{\nu}_{k0}$, the potential displacements Δ_i^k along the ith dimensionless normal coordinates ($i = 1,2$, $k = 1,2,3$), n_c (the number density of the pigment molecule in microcrystal) and l (the depth in the disc) were required. For simplicity, we assumed $\nu_i^{(0)} = \nu_i^{(k)} = \nu_i$ and the displacement Δ_i^k were the same for $k = 1,2,3$ (i.e., $\Delta_i^1 = \Delta_i^2 = \Delta_i^3 \equiv \Delta_i$). We took the values of s and s' as 510 cm^{-1} and 340 cm^{-1}, respectively (the values well reproduced the average line width of the experimental RREPs). We put $\overline{\nu}_{10} = 14,200\ cm^{-1}, \overline{\nu}_{20} = 17,600\ cm^{-1}, \overline{\nu}_{30} = 19,700\ cm^{-1}$ from Fig. 1.

The values of ν_i and $\Delta_i (i = 1,2)$ were fixed such parameters as $\nu_1 = 1520\ cm^{-1}, \nu_2 = 1150\ cm^{-1}, \Delta_1 = 1.2$, and $\Delta_2 = 1.0$, since the overall shapes of RREPs do not depend so much on theses values. The value of d_{30} was taken to be 15.65 D (Debye) from the absorption spectrum [13]. However, the value of d_{20} has not yet been obtained from absorption spectrum. Nevertheless, from the fluorescence quantum yields [13,19], the values of $d'_{20} = 4.54$ D together with $d'_{10} = 0.72$ D have been obtained. Here, the prime attached to d_{k0} denotes that its value was obtained from fluorescence measurement. Absorption spectra of various carotenoids for the $2A_g^- \leftarrow 1A_g^-$ transition region have been reported by Wang et al. [20]. In particular, the $2A_g^-(\vec{v}=\vec{0}) \leftarrow 1A_g^-(\vec{u}=\vec{0})$ vibronic band for spirilloxanthin was clearly seen at 12,740 cm^{-1} and the ratio of the molar extinction coefficient of the $2A_g^-(\vec{v}=\vec{0}) \leftarrow 1A_g^-(\vec{u}=\vec{0})$ peak to that of the $1B_u^+(\vec{v}=\vec{0}) \leftarrow 1A_g^-(\vec{u}=\vec{0})$ peak was reported to be about 4×10^{-4}; from the value, assuming their band widths are equal, we could estimate the transition dipole moment between $2A_g^-$ and $1A_g^-$ states to be *0.73* D. (Frank–Condon factors were calculated using the values $\Delta_1^1 = 1.2$, $\Delta_2^1 = 1.9, \Delta_1^3 = 1.2$ and $\Delta_2^3 = 1.0$.) The transition dipole moment thus calculated is about one-half of the transition dipole moment obtained from fluorescence measurement, i.e., 1.37 D [19], suggesting that the deviation from the $C_{2\,h}$ symmetry in the equilibrium nuclear configuration in the excited state is much larger than that in the

ground state. Assuming the same ratio for the transition dipole moments d_{10} and d_{20} in spheroidene, i.e., $d_{10}/d'_{10} = d_{20}/d'_{20} = 0.73\ \mathrm{D}/1.37\ \mathrm{D}$, we set $d_{10} = 0.38$ D and $d_{20} = 2.41$ D.

Reliable values of $\gamma_{k0}(k = 1,2,3)$ in low temperatures are not available at present. The molarity of spheroidene in the microcrystal was estimated to be 1.75 M, assuming its specific gravity to be 1.0. From this, we put $n_c = 1.05 \times 10^{21}\ \mathrm{cm}^{-3}$. The depth in the disc, l, was set to 0.5 mm according to the experimental condition.

Fig. 4 (a) shows a simple model calculation of r_k $(k = 1,2,3)$ (Eq. (7)) for spheroidene as a function of the size a. The values of $\bar{\sigma}_k$ $(k = 1,2,3)$, needed in Eq. (7), were taken as follows: $\bar{\sigma}_3$ was determined to be 6.26 Å^2 by using the value of $\epsilon = 1.64 \times 10^5$ at $\nu = \bar{\nu}_{30}$ [13]. $\bar{\sigma}_1$ and $\bar{\sigma}_2$ were calculated to be 0.0027 Å^2 and 0.13 Å^2, respectively, by using the formula $\bar{\sigma}_k = (\bar{\nu}_{k0}/\bar{\nu}_{30})(d_{k0}/d_{30})^2\bar{\sigma}_3$. It can be seen from Fig. 4 (b) that the ratio $r_1/r_3(r_2/r_3)$ varies from 1 to 42.0 (6.9) as the size of microcrystal increases from zero to 50 μm. Optical microscopy gave us rough images of microcrystals (pigment aggregates) of tens of μm in diameter (Fig. 2), and it is difficult to estimate the average size of microcrystals unambiguously. Furthermore, the values of γ_{k0}/γ_{30} are unknown. Thus, we took the values of $(r_k/r_3)(\gamma_{k0}/\gamma_{30})^{-1/2}$ $(k = 1,2)$ as fitting parameters. (The overall feature of RREPs does not depend on respective values of $r_k\gamma_{k0}^{-1/2}$, but depends only on their ratios.).

By using thus-estimated values of parameters, i.e., $s, s', \nu_i, \Delta_i, \bar{\nu}_{k0}$ and d_{k0}, we found that when the value of $(r_1/r_3)(\gamma_{10}/\gamma_{30})^{-1/2} = 140$ and that of $(r_2/r_3)(\gamma_{20}/\gamma_{30})^{-1/2} = 12$, the best agreement between the simulated RREPs and the observed ones was obtained for the overall concentrations (a) 1.6×10^{-5} M and (b) 8×10^{-3} M; we also found that when we set the concentration to be less than 1.75×10^{-1} M, Eq. (24) could reproduce the observed RREPs for (c) spheroidene crystals in a film fairly well, though the observed RREPs were obtained in the grazing-incidence geometry (Figs. 1 and 5). If we assume the average size of microcrystals to be 20 μm, Eq. (7) gives a value of 31.7 (6.9) for r_1/r_3 (r_2/r_3). Then we can estimate the values of $(\gamma_{10}/\gamma_{30})^{-1/2}$ and $(\gamma_{20}/\gamma_{30})^{-1/2}$ to be 4.49 and 1.76, showing that the RR scattering efficiency of microcrystal plays an essential role $(r_k^2/r_3^2 \gg \gamma_{k0}/\gamma_{30})$.

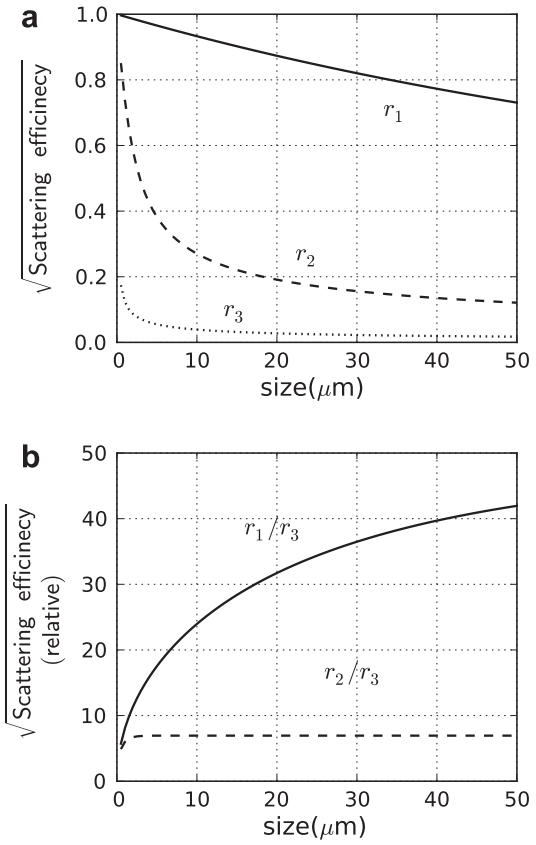

Fig. 4. (a) Square root of the resonance-Raman scattering efficiencies r_1, r_2 and r_3 of a microcrystal of spheroidene as functions of it's size (in μm) for the $S_1(2A_g^-)$ state (full line), the $S_2(1B_u^-)$ state (dashed line) and the $S_3(1B_u^+)$ state (dotted line), respectively. (b) Relative values of r_1 (full line) and r_2 (dashed line) with respect to r_3 as functions of the microcrystal's size.

4. Discussion and conclusion

We have formulated an expression for RREPs due to the Albrecht A-term of pigment aggregates dispersed in KBr disc, taking into account the first and second kinds of self-absorptions of incident and scattered light. Based on the resultant formula, the RREPs of spheroidene were simulated and fairly good agreement between the observed and the simulated RREPs were obtained for the values of $d_{10} = 0.38$ D, $d_{20} = 2.41$ D and $d_{30} = 15.65$ D, (see Figs. 1 and 5).

The value of $d_{20}(|d_{20}/d_{30}|^2 = 2.4 \times 10^{-2})$ might be somewhat larger than the true value judging from the absorption spectrum of spheroidene in solution [20]. However, the breakdown of the C_{2h} symmetry of the molecule due to a static distortion in the microcrystals may produce such value of transition dipole moment, by adding some value to the original one [9]. Furthermore, if we take the d_{20} value of 1.56 D $(|d_{20}/d_{30}|^2 = 1.0 \times 10^{-2})$, a choice of a set of

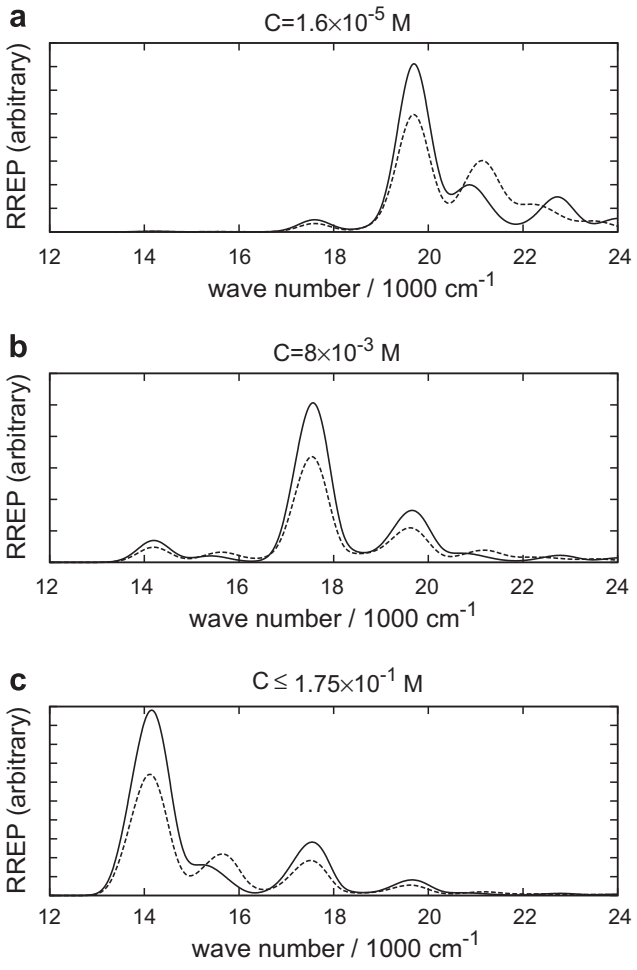

Fig. 5. Simulated resonance-Raman excitation profiles of the C=C (full line) and the C—C (dashed line) stretching modes for spheroidene in KBr disc at overall concentrations (a) 1.6×10^{-5} M, (b) 8.0×10^{-3} M and (c) $\lesssim 1.75 \times 10^{-1}$ M. In the simulation, aggregates of spheroidene molecules are dispersed in the disc with its average size being 20 μm (see text).

values of $(r_1/r_3)(\gamma_{10}/\gamma_{30})^{-1/2} = 140$ and $(r_2/r_3)(\gamma_{20}/\gamma_{30})^{-1/2} = 6$ reproduced almost the same simulated RREPs as those in Fig. 5 (data not shown), and it has been shown that the following argument does not depend on the value of d_{20} if it satisfies the condition $d_{10} \ll d_{20} \ll d_{30}$. Thus, in the following we will use the value of $d_{20} = 2.41$ D.

Now, let us investigate the mechanism mentioned in Introduction, based on our theory described in Section 2 and the result of simulations in Section 3. Eq. (24) together with Eq. (17) tells us that there are the following four factors which determine the magnitude of RREP of the C=C or C—C mode at $\nu = \bar{\nu}_{k0}$, which we denote by $I^{(k)}_{i\vec{0}}$:

(i) the fourth power of the transition dipole moment, i.e., $|d_{k0}|^4$,
(ii) the inverse of homogeneous dephasing constant for the electronic coherence between S_k and S_0, i.e., γ^{-1}_{k0},
(iii) the RR scattering efficiency of microcrystal, r_k^2, which is associated with the first kind of self-absorption, and
(iv) the factor due to the second kind of self-absorption, which can be measured by the quantity $[1-\exp(-\tilde{\sigma}_k\bar{n}l)]/\tilde{\sigma}_k \equiv A_k$, where $\tilde{\sigma}_k = 4\pi^2\ \bar{\nu}_{k0}|d_{k0}|^2/(3\hbar c)$.

(Note that the RR scattering associated with the $S_k(\vec{\nu}=\vec{0}) \leftarrow S_0(\vec{u}=\vec{0})$ transition is not self-absorbed since there is no absorption band at the longer-wavelength side of the $S_k(\vec{\nu}=\vec{0}) \leftarrow S_0(\vec{u}=\vec{0})$ absorptive transition.) The factors due to the second kind of self-absorption, A_k, are obtained for three different overall concentrations as (a) $A_1 = 1.00$, $A_2 = 1.00$, $A_3 = 0.86$ for $C = 1.6\times10^{-5}$ M, (b) $A_1 = 0.97$, $A_2 = 0.32$, $A_3 = 6.9\times10^{-3}$ for $C = 8\times10^{-3}$ M, and (c) $A_1 = 0.53$, $A_2 = 1.4\times10^{-2}$, $A_3 = 3.0\times10^{-4}$ for $C \lesssim 1.75\times10^{-1}$ M.

When a pigment molecule (taking the same nuclear configuration as in microcrystals) is placed in vacuum, the RR scattering intensity, $I^{(k)}_{i\vec{0}}$, is proportional to $|d_{k0}|^4\gamma^{-1}_{k0}$ so that $I^{(1)}_{i\vec{0}} : I^{(2)}_{i\vec{0}} : I^{(3)}_{i\vec{0}} = 0.42 : 104 : 59,990$ (γ_{30} is set to 1). When the pigment molecules aggregate in microcrystals, on the other hand, the RR scattering intensity (per molecule), $I^{(k)}_{i\vec{0}}$, is proportional to $|d_{k0}|^4 r_k^2\gamma^{-1}_{k0}$ and, as a result, we have $I^{(1)}_{i\vec{0}} : I^{(2)}_{i\vec{0}} : I^{(3)}_{i\vec{0}} = 0.32 : 3.81 : 47.0$. Here, $I^{(3)}_{i\vec{0}}$ is substantially reduced but still larger than $I^{(2)}_{i\vec{0}}$.

When the microcrystals are dispersed in a KBr disc, $I^{(k)}_{i\vec{0}}$ is proportional to $|d_{k0}|^4 r_k^2\gamma^{-1}_{k0}A_k$. For three different overall concentrations, the ratios of the RR scattering intensities were obtained as follows: $I^{(1)}_{i\vec{0}} : I^{(2)}_{i\vec{0}} : I^{(3)}_{i\vec{0}} = 0.32 : 3.80 : 40.6$ for $C = 1.6\times10^{-5}$ M, $I^{(1)}_{i\vec{0}} : I^{(2)}_{i\vec{0}} : I^{(3)}_{i\vec{0}} = (0.31 : 1.2 : 0.32$ for $C = 8\times10^{-3}$ M and $I^{(1)}_{i\vec{0}} : I^{(2)}_{i\vec{0}} : I^{(3)}_{i\vec{0}} = 0.17 : 0.055 : 0.014$ for $C = 1.75\times10^{-1}$ M. These estimations show that (1) at the lowest concentration, no (second kind of) self-absorption takes place and $I^{(3)}_{i\vec{0}}$ is dominant over $I^{(2)}_{i\vec{0}}$ and $I^{(1)}_{i\vec{0}}$, and (2) at the medium concentration, the (second kind of) self-absorption suppresses $I^{(3)}_{i\vec{0}}$ selectively and then $I^{(2)}_{i\vec{0}}$ becomes dominant over $I^{(3)}_{i\vec{0}}$ and (3) at the highest concentration, the (second kind of) self-absorption suppresses $I^{(2)}_{i\vec{0}}$ and $I^{(3)}_{i\vec{0}}$ selectively and then $I^{(1)}_{i\vec{0}}$ becomes dominant over $I^{(2)}_{i\vec{0}}$ and $I^{(3)}_{i\vec{0}}$.

Before coming to a conclusion, let us consider the mechanism that has been proposed by Hashimoto et al. [9]. They started with the follwoing equation, which follows from Eq. (10) by the replacement of r_k and γ_{k0} by *1* and $\gamma_k/2$, respectively,

$$S_{i\vec{0}}(\nu) = \frac{1}{9h^2c^2}\sum_k\sum_{\vec{\nu}} d_{k0}^4 \frac{\left|\left\langle\chi^{(0)}_{\vec{u}}|\chi^{(k)}_{\vec{\nu}}\right\rangle\left\langle\chi^{(k)}_{\vec{\nu}}|\chi_{\vec{0}(0)}\right\rangle\right|^2}{\left(\nu_{k0}+\vec{\nu}^{(k)}\cdot\vec{\nu}-\nu\right)^2+\gamma_k^2/4}. \tag{25}$$

Taking into account the (second kind of) self-absorption effect, they obtained from this in our notations

$$I^{(3)}_{i\vec{0}}/I^{(1)}_{i\vec{0}} = [(f_{30}/f_{10})(\nu_{10}/\nu_{30})(\gamma_1/\gamma_3)]^2[\sigma(\nu_{30})/\sigma(\nu_{10})], \tag{26}$$

where f_{10} and f_{30} are the oscillator strengths (note that $f_{k0} \propto \nu_{k0}\ d_{k0}^2$). Based on this equation, they explained the relative intensities of the observed C=C mode RREP peaks $\left(I^{(3)}_{i\vec{0}}/I^{(1)}_{i\vec{0}}\right)$ for β-carotene in randomly oriented crystals by using the values of $f_{10} = 0.01$ ($d_{10} = 1.8$ D), $f_{30} = 1$, $\nu_{10}/\nu_{30} = 14{,}500/18{,}400$ and $\gamma_1/\gamma_3 = (150\times10^{-15})/(10\times10^{-12}) = 0.015$. The origin of the large value of f_{10} was attributed to the symmetry degradation of the molecule in the crystal. Now, if we assume that Eq. (25) can be applied to the present observations, then the FWHM of RREP associated with $S_3 \leftarrow S_0$ transition should be at least 67(=1/0.015) times larger than that associated with $S_1 \leftarrow S_0$ transition. However, this is obviously not the case as Fig. 1 shows. Thus, in addition to the second kind of self-absorption and the symmetry degradation, another mechanism is necessary.

Two-step self-absorption mechanism: In conclusion, from the above analysis we get an answer to the question what mechanism enables formally optically-forbidden $2A_g^-$ and $1B_u^-$ states to be observed in RREPs, free from the contribution of optically-allowed $1B_u^+$ state. The mechanism consists of two steps. The first step is the aggregation of pigment molecules to form a microcrystal. When the size of microcrystal is larger than several μm, the RR scattering associated with the $1B_u^+ \leftarrow 1A_g^-$ transition is substantially reduced as compared to that associated with $1B_u^- \leftarrow 1A_g^-$ or $2A_u^- \leftarrow 1A_g^-$ transition due to the (first kind of) self-absorption within microcrystal (Fig. 4). The second step is the random dispersion of the aggregated pigments in a KBr disc. At a medium overall

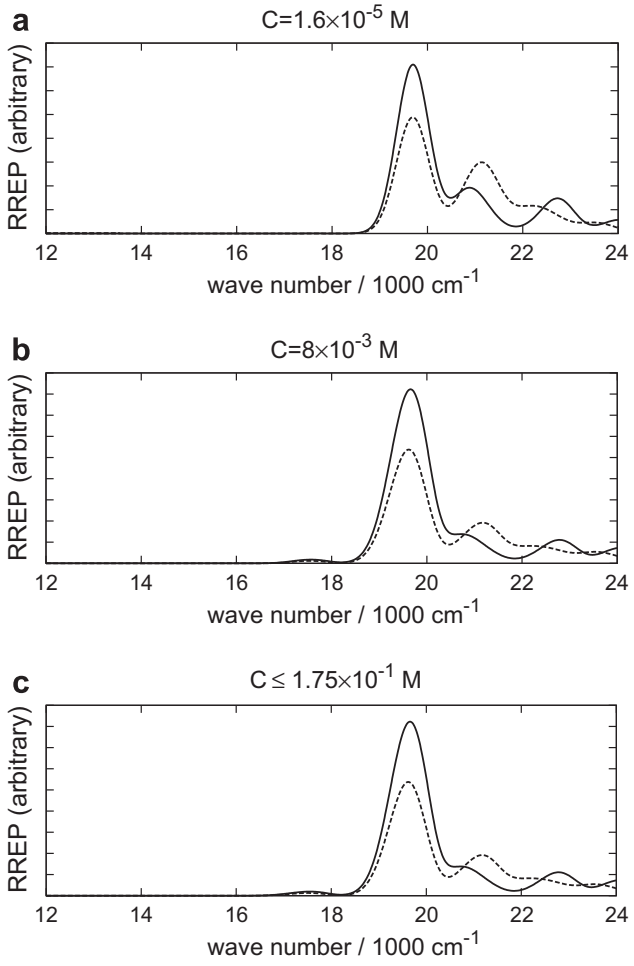

Fig. 6. Simulated resonance-Raman excitation profiles of the C=C (full line) and the C—C (dashed line) stretching modes for spheroidene in KBr disc at concentrations (a) 1.6×10^{-5} M, (b) 8.0×10^{-3} M and (c) $\lesssim1.75\times10^{-1}$ M. In the simulation, spheroidene molecules are dispersed uniformly in the disc.

concentration, the self-absorption by other microcrystals, i.e., the second kind of self-absorption, suppresses the RR scattering from $1B_u^+ \leftarrow 1A_g^-$ transition selectively, and as a result, the RR scattering from $1B_u^- \leftarrow 1A_g^-$ prevails over that from $1B_u^+ \leftarrow 1A_g^-$. At a higher overall concentration, the (second kind of) self-absorption suppresses the RR scattering from both $1B_u^+ \leftarrow 1A_g^-$ and $1B_u^- \leftarrow 1A_g^-$ transitions, leading to the selective observation of the RR scattering from the $2A_g^- \leftarrow 1A_g^-$ transition. Both steps are equally important; only one step cannot reproduce the experimental results even qualitatively. Fig. 6 displays the result of simulation of the C=C and C—C RREPs for spheroidene when the molecules are dispersed uniformly in KBr disc. This result demonstrates that the aggregation of molecules is essential for the $2A_g^-$ and $1B_u^-$ RREPs to be observed.

Fairly good agreement seen between the simulated RREPs of the C=C and C—C modes by the use of appropriate parameters and the experimentally-determined RREPs for spheroidene in KBr disc at a concentration of $C = 8 \times 10^{-3}$ M corroborates the presence of the electronic excited state $1B_u^-$ between the $2A_g^-$ and $1B_u^+$ states in energy.

Further investigation by the use of specifically determined size of microcrystals, however, will be necessary to quantitatively establish the present mechanism.

Acknowledgement

The authors thank Dr. K. Furuichi for offering photographs of microcrystals of carotenoids in KBr disc.

References

[1] A. Young, G. Britton (Eds.), Carotenoids in Photosynthesis, Chapman and Hall, London, 1993.
[2] T. Polívka, V. Sundström, Chem. Rev. 104 (2004) 2021.
[3] A. Damjanović, T. Ritz, K. Schulten, Phys. Rev. E 59 (1999) 3293.
[4] B. Hudson, B. Kohler, Ann. Rev. Phys. Chem. 25 (1974) 437.
[5] P. Tavan, K. Schulten, J. Chem. Phys. 85 (1987) 6602.
[6] Y. Kurashige, H. Nakano, Y. Nakao, K. Hirao, Chem. Phys. Lett. 400 (2004) 425.
[7] T. Sashima, H. Nagae, M. Kuki, Y. Koyama, Chem. Phys. Lett. 299 (1999) 187.
[8] K. Gaier, A. Angerhofer, H.C. Wolf, Chem. Phys. Lett. 187 (1991) 103.
[9] H. Hashimoto, Y. Koyama, Y. Mori, Jpn. J. Appl. Phys. 36 (1997) L916.
[10] T. Sashima, M. Shiba, H. Hashimoto, H. Nagae, Y. Koyama, Chem. Phys. Lett. 290 (1998) 36.
[11] J. Tang, A.C. Albrecht, in: H.A. Szymanski (Ed.), Raman Spectroscopy, vol. 2, Plenum, New York, 1970.
[12] K. Onaka, R. Fujii, H. Nagae, M. Kuki, Y. Koyama, Y. Watanabe, Chem. Phys. Lett. 315 (1999) 75.
[13] J.-P. Zhang, R. Fujii, P. Qian, T. Inaba, T. Mizoguchi, Y. Koyama, K. Onaka, Y. Watanabe, H. Nagae, J. Phys. Chem. B 104 (2000) 3683.
[14] W.W. Parson, Modern Optical Spectroscopy, Springer-Verlag, Heidelberg, 2008.
[15] S. Mukamel, Principles of Nonlinear Optical Spectroscopy, Oxford University Press, Oxford, 1995.
[16] A. Gilbert, J.E. Baggott, Essentials of Molecular Photochemistry, Blackwell Science Inc, London, 1991.
[17] J. Olivero, R. Longbothuma, J. Quant. Spectrosc. Radiat. Transfer 17 (1977) 233.
[18] V.B. Berestetskii, E.M. Lifshitz, L.P. Pitaevskii, Quantum Electrodynamics, Pergamon Press, New York, 1982.
[19] R. Fujii, T. Ishikawa, Y. Koyama, M. Taguchi, Y. Isobe, H. Nagae, Y. Watanabe, J. Phys. Chem. A 105 (2001) 5348.
[20] P. Wang, R. Nakamura, Y. Kanematsu, Y. Koyama, H. Nagae, T. Nishio, H. Hashimoto, J.-P. Zhang, Chem. Phys. Lett. 410 (2005) 108.